Proceedings of the Seventh International Conference on
Railway Technology: Research, Development and Maintenance
Edited by: J. Pombo
Civil-Comp Conferences, Volume 15, Paper 11.9
Civil-Comp Press, Edinburgh, United Kingdom, 2026
ISSN: 2753-3239, doi: 10.4203/ccc.15.11.9

Analysis of a Novel Levitation Magnet for High-Speed Maglev Train

S. Fu[1,2], Y. Zhou[1,2] and W. Han[1,2]

[1]CRRC Qingdao Sifang Co., Ltd., China
[2]State Key Laboratory of High-speed Maglev Transportation Technology, China

Abstract

The levitation electromagnet is the core component for providing levitation force in high-speed maglev trains. This paper proposes a novel structure and power supply scheme for suspension electromagnets, where the coil is split into a regulating coil (connected to a controller) and a constant-current coil (supplied by a constant-current source). First, the circuit, magnetic circuit, and internal heat transfer models of the electromagnet are established to analyze its power loss, electromagnetic force, and temperature characteristics. Then, the coil turns and supply current are optimized with the maximum electromagnetic force-to-power ratio as the objective. Finally, a finite element model is constructed to compare the proposed electromagnet with the conventional one, verifying the feasibility of the novel structure and power supply scheme. This study provides a reliable reference for the design and optimization of high-speed maglev suspension electromagnets.

Keywords: high-speed maglev train, levitation magnet, thermal network model, electromagnetic model, force-to-power ratio, temperature characteristics.

1 Introduction

Maglev train is a new type of rail transit. It is safe, reliable, adaptable, quiet, comfortable and environment-friendly. So far, maglev train technology has been studied by many countries, such as China, Germany, Japan, South Korea, etc, see Smith[1-3]. According to operating speeds, the maglev train can be classified into middle–low- and high-speed types. The maximum speed of the middle–low-speed maglev train approaches 200 km/h. A U-type magnet has been designed to achieve integrated levitation and guidance. Here, the levitation is actively controlled to maintain stability and the guidance is passive due to smaller lateral interference forces at lower speeds, see Smith [4-6]. The maximum speed of the high-speed maglev trains is over 300 km/h, even reaching 600 km/h. At present, there are main two technical routes: superconducting electrodynamic suspension (SCEDS) vehicles from Japan and electromagnetic suspension (EMS) Transrapid technology from Germany. SCEDS vehicles achieve passive levitation and guidance via the passive repulsive forces generated by the dynamic interaction between the superconducting magnets and the ground coils. It is crucial to design the superconducting magnet itself and match the relationship with the ground coils to ensure stable levitation, see Smith [7-9]. The SCEDS vehicle L0 in Japan is in the trial operation stage and its maximum experiment speed reaches 603 km/h, but it is not available commercially yet. At present, the technical route of EMS is most mature and the EMS Transrapid TR08 manufactured by German firms has been operating commercially for nearly 20 years in Shanghai, China. The maximum experiment speed reaches 505 km/h and the maximum operation speed reaches 430 km/h. The levitation and guidance functions are achieved through active magnetic attraction forces generated by corresponding magnets, which are dynamically controlled to ensure stability, especially under the significant vertical and lateral loads experienced at high speeds , see Smith [10-12].The levitation magnet of constant conduction high -speed maglev uses DC power supply to establish magnetic field and the magnetic poles are made of multiple coils of aluminum foil wrapped around the iron core, see Smith [13]. Therefore, the dynamic response of the magnetic pole is relatively slow. In addition, the long-term operation of the levitation magnet will produce high power loss, resulting in a rise in the temperature, see Smith [4]. Levitation magnets are prone to surface thermal cracks when working at high temperatures for a long time. The overall insulation performance of the levitation magnet is affected, and the safety and stability of the maglev train are seriously reduced, see Smith [15-17].

This paper presents a novel electromagnet structure and power supply scheme for high-speed maglev trains featuring a maximum force-to-power ratio. Each magnetic pole consists of mutually independent constant-current coils and regulation coils. The constant-current coils are powered by a DC source, while the regulation coils are controlled by the levitation controller to accomplish vehicle levitation. By optimizing the control strategies and turn allocation schemes of the constant-current and regulation coils, the ratio of electromagnetic force to power at the rated operating point of the normal-conducting high-speed maglev pole is reduced by 2.8%, and the temperature rise is decreased by 9.7 K under static no-wind conditions and by 27 K under dynamic wind conditions.

2 Structure and Model

2.1 Structure

The physical model of the levitation electromagnet and the long stator for high-speed maglev trains is illustrated in Figure 1.The levitation electromagnet contains 12 magnetic poles with alternating N and S polarities.Each pole consists of a coil, an iron core, and a yoke, with adjacent poles connected by the yoke.When energized, the poles generate a magnetic field that interacts with the magnetic field of the long stator to produce electromagnetic attractive force, thus achieving levitation.

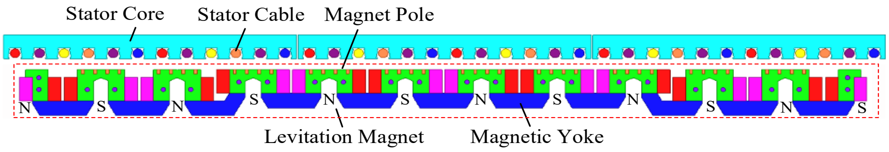

Figure 1: Physical model of the levitation magnet.

As a key component in the active excitation of the magnet, the magnetic pole is shown in Figure 2, which comprises an iron core, coils, an insulating layer, a linear induction generator (LIG), and a flange. Similar to the yoke, the iron core is constructed of laminated silicon steel sheets.The upper and lower coils are connected and wound around the iron core,composed of alternately arranged aluminum foils and insulating films.

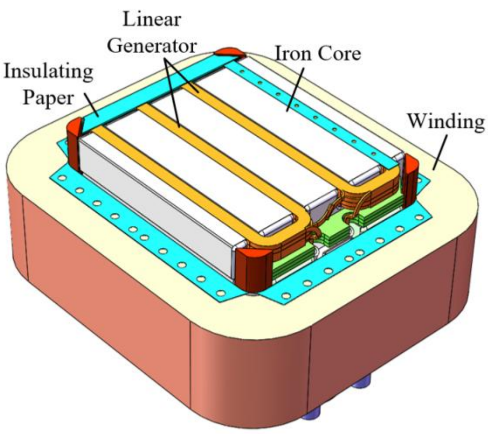

Figure 2: Schematic diagram of magnetic pole structure.

The conventional electromagnet consists of 12 magnetic poles, divided into left and right groups with six poles in each group. For electrical connection, the upper and lower coils of each pole are first connected in series to form a pole unit.Subsequently, the six pole units within the same group are connected in series in sequence to form a power supply loop.Each loop is connected to the corresponding levitation controller, enabling independent regulation and control by individual controllers, as shown in Figure 3.

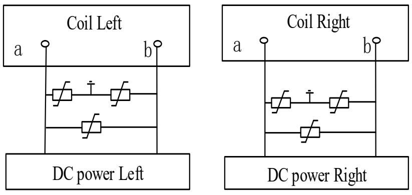

Figure 3: Schematic diagram of power supply for the conventional electromagnet.

The novel electromagnet still comprises 12 magnetic poles with alternating N and S polarities.However, a separated coil configuration is adopted for the magnet of the proposed electromagnet, as illustrated in Figure 4. Among the six magnetic poles on each side, the lower coils of all poles are directly connected in series to form a constant-current coil loop, which is connected to a constant-current source to provide stable basic levitation force for the train.Meanwhile, the upper coils of all poles on the same side are directly connected in series to form an regulation coils loop, which is linked to the levitation controller to regulate the current in real time according to external excitations, thereby dynamically controlling the levitation force to achieve stable operation. Accordingly, the novel electromagnet contains four power supply loops in total, namely the left constant-current loop, left control loop, right constant-current loop, and right control loop.Each loop is connected in series with the six magnetic pole coils on the same side, and the power supply loops are shown in Figure 5.

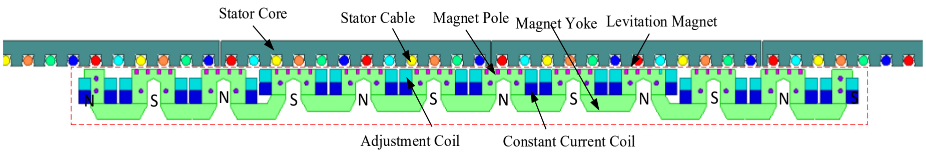

Figure 4: Schematic diagram of the novel electromagnet structure.

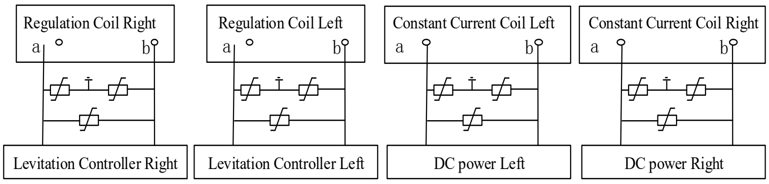

Figure 5: Schematic diagram of power supply for the novel electromagnet.

2.2 Circuit Model

The regulation coil is powered by the levitation controller. The output of the controller is the voltage, which is converted to the corresponding load current according to the load characteristics of the control loop. The circuit model of the levitation magnet is constructed to analyze the response speed of the levitation magnet, see Smith [18]. The series connection of the regulation coil of half a magnet can actually be equivalent to the series connection of 6 resistors and 6 inductors, as shown in Figure 6.

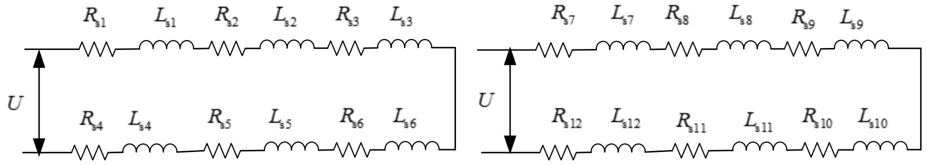

a) Regulation coil

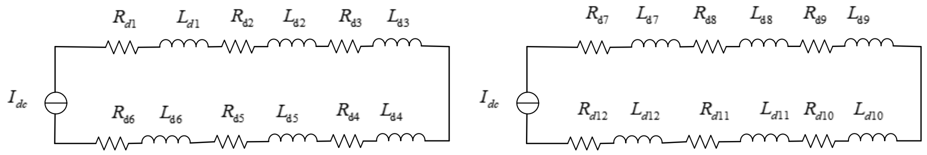

b) Constant Current Coil

Figure 6: Schematic diagram of magnet power supply.

In Figure 6, R_{sj} represents the resistance of a single magnetic pole regulation coil; L_{sj} is the inductance of a single magnetic pole regulation coil; U is the input voltage of the regulation coil control circuit. R_{dj} is the resistance of a single pole constant current coil; L_{dj} is the inductance of a single pole constant current coil; I_{dc} is the input current of the constant current coil.

The power loss of a magnet mainly refers to the energy loss caused by the heating of the magnetic pole coil, including the power loss P_d of the constant current coil and the power loss P_s of the regulation coil, as shown in Equation (1). Its size is related to current and resistance.

$$P = P_s + P_d = I(t)^2 \sum R_{sj} + I_{dc}{}^2 \sum R_{dj} \tag{1}$$

2.3 Magnetic Circuit Model

Taking the regulation coil as an example, a half magnet equivalent magnetic circuit model is constructed as shown in Figure 7 The magnetic circuit includes air gap magnetic resistance, leakage magnetic resistance, and magnetic material magnetic resistance, see Smith [19-21]. In the figure, Yaj represents the air gap reluctance between the magnetic pole and the long stator; Ysi is the magnetic resistance of the long stator core; Yei represents the magnetic pole core and magnetic yoke reluctance; Yli is the leakage magnetic resistance between adjacent magnetic poles; ϕaj, ϕsi, ϕei and ϕli represents the magnetic flux corresponding to the magnetic resistances Yaj, Ysi, Yei and Yli, respectively; θi is the magnetic pole electromotive force NI, N is the number of turns of the magnetic pole regulation coil, and I is the current of the regulation coil circuit; i=1,2，…， 5；j=1,2，…， 6.

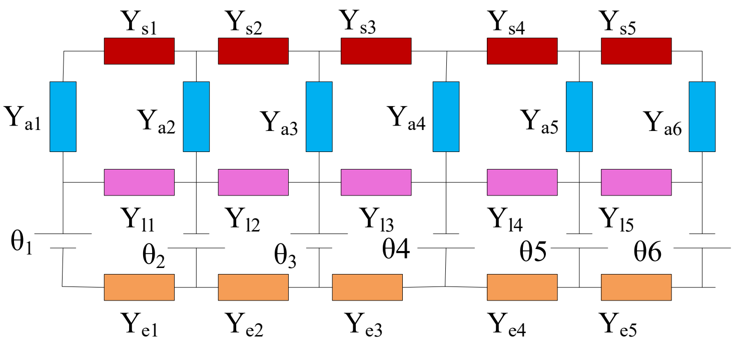

Figure 7: Equivalent magnetic circuit model of half electromagnet.

According to Kirchhoff's voltage law, a system of equations regarding magnetic flux is established, as shown in Equation (2).

$$\begin{cases} Y_{ai}\phi_{ai} + Y_{si}\phi_{si} + Y_{ai}\phi_{ai} + Y_{ei}\phi_{ei} = \theta_i + \theta_{i+1} \\ Y_{ei}\phi_{ei} + Y_{li}\phi_{li} = \theta_i + \theta_{i+1} \end{cases} \tag{2}$$

Due to the influence of the slot structure of the magnetic pole linear generator (LIG) and the long stator tooth slot, the air gap magnetic flux distribution between the magnetic pole and the long stator is relatively complex, as shown in Figure 8. Therefore, the air gap flux is equivalently divided into main flux, slot flux, and LIG flux, see Smith [22-23]. The three types of magnetic flux correspond to the corresponding magnetic resistance.

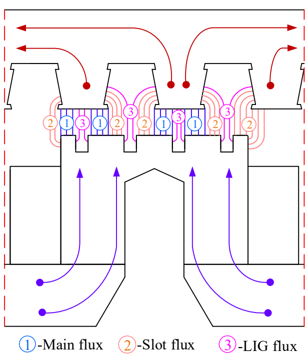

Figure 8: Air gap magnetic field distribution.

The air gap reluctance is a combination of three types of reluctance in parallel, as shown in Equation (3).

.

$$\frac{1}{Y_{aj}} = \frac{1}{Y_{amj}} + \frac{1}{Y_{anj}} + \frac{1}{Y_{aLi}} \tag{3}$$

where: Y_{amj} is the main magnetic flux corresponding to the reluctance; Y_{anj} is the magnetoresistance corresponding to the slot flux. Y_{aLj} is the magnetoresistance corresponding to the LIG flux. Each reluctance can be calculated by Equation (4).

$$\begin{cases} Y_{amj} = \dfrac{s_j + h_{mj}}{\mu_0 A_{amj}} \\ Y_{anj} = \dfrac{s_j + h_{nj}}{\mu_0 A_{anj}} \\ Y_{aLj} = \dfrac{s_j + h_{Lj}}{\mu_0 A_{aLj}} \end{cases} \tag{4}$$

where: s_j is the gap between the magnetic pole and the long stator teeth; μ_0 is the permeability of air. A_{amj}, A_{anj} and A_{aLj} are the main flux, slot flux and air gap area of LIG respectively. The extra air gap length of h_{mj}, h_{nj} h_{Lj} are the main flux, slot flux and LIG flux respectively. The magnetic flux of each part of the air gap is in Equation (5)

$$\begin{cases} \phi_{amj} = \dfrac{\phi_{aj} Y_{aj}}{Y_{amj}} \\ \phi_{anj} = \dfrac{\phi_{aj} Y_{aj}}{Y_{anj}} \\ \phi_{aLj} = \dfrac{\phi_{aj} Y_{aj}}{Y_{aLj}} \end{cases} \tag{5}$$

Based on the principle of virtual work, the electromagnetic force corresponding to each part of the air gap is in Equation (6).

$$\begin{cases} F_{mj} = \dfrac{\phi_{amj}^{\ 2}}{2\mu_0 A_{amj}} \\ F_{nj} = \dfrac{\phi_{anj}^{\ 2}}{2\mu_0 A_{anj}} \\ F_{Lj} = \dfrac{\phi_{aLj}^{\ 2}}{2\mu_0 A_{aLj}} \end{cases} \tag{6}$$

The electromagnetic force of a single pole regulation coil is the sum of the electromagnetic force of all parts, that is in Equation (7)

$$F = F_{mj} + F_{nj} + F_{Lj} \tag{7}$$

Similarly, the electromagnetic force of the constant current coil can be obtained.

2.4 Thermal Network Model of Magnetic Pole

Based on the structural symmetry of the magnetic pole, a thermal network model of half the magnetic pole is established.The contact thermal resistances at different interfaces, including those of the magnetic pole core and encapsulation resin, are calculated respectively.For the coil structure with alternately arranged aluminum foils and insulating films, the coil is divided into multiple layers along the high-thermal-resistance direction, and the equivalent thermal resistance of each layer is computed individually.

The heat transfer paths involve thermal conduction and convection resistances, while thermal radiation resistance is neglected.The thermal network model according to the contact thermal resistances at various positions is illustrated in Fig. 8.P_1–P_3 denote the thermal resistances of the magnetic pole core;P_4–P_{11} represent the thermal resistances of the coil structure with alternating foils and insulating films;P_{12}–P_{21} correspond to the thermal resistances of the pole resin. In Equation (8), the formulation can be derived from the governing equation of unsteady heat conduction.

$$c_p m_p \frac{dT_p}{dt} = \sum_p D_{k,p}(T_p - T_k) + \sum_p C_p(T_p - T_0) + Q_p, p = 1,2,3,\cdots 21; \quad k = 1,2\cdots 21; \tag{8}$$

In Equation (8), c_p is the specific heat capacity at node p, m_p is the mass of the component, T_p is the temperature at node p, and t denotes time. $D_{k,p}$ represents the thermal conduction coefficient between node k and node p, and T_k is the temperature at node k. C_p is the convective heat transfer coefficient between node p and air, and T_0 stands for the ambient temperature. Q_p is the power consumption of node p.The formula for calculating $D_{k,p}$ is given in Equation (9).

$$D_{k,p} = \frac{\lambda_k A_{k,p}}{\delta_{k,p}} \tag{9}$$

where λ_k is the thermal conductivity of node k, $A_{k,p}$ is the contact area between node k and node p, and $\delta_{k,p}$ is the heat conduction distance between node k and node p.

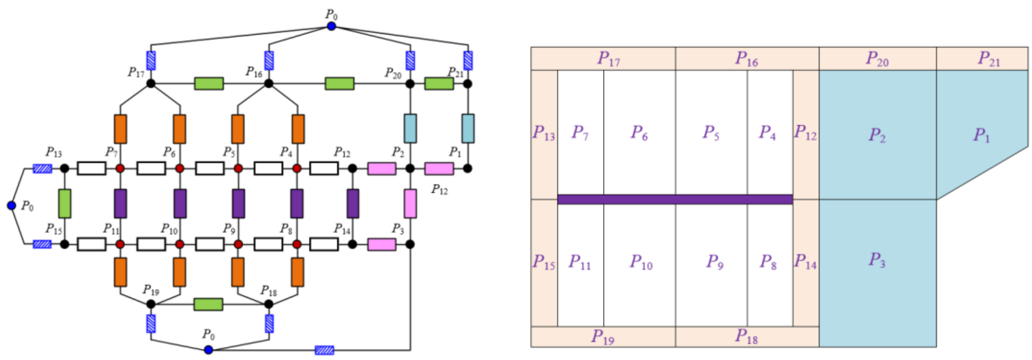

Figure 9: Air gap magnetic field distribution.

A system of equations regarding thermal resistance is established in the thermal network, as shown in Equation (10) .

$$
\begin{cases}
c_1 m_1 \dfrac{dT_1}{dt} = D_{1-21}(T_{21} - T_1) + D_{1-2}(T_2 - T_1) \\
c_2 m_2 \dfrac{dT_2}{dt} = D_{1-2}(T_1 - T_2) + D_{2-20}(T_{20} - T_2) + D_{2-12}(T_{12} - T_2) + D_{2-3}(T_3 - T_2) \\
\vdots \\
c_{21} m_{21} \dfrac{dT_{21}}{dt} = D_{20-21}(T_{20} - T_{21}) + D_{1-21}(T_1 - T_{21}) + D_{21-0}(T_{21} - T_0)
\end{cases} \tag{10}
$$

The temperatures at various positions inside the magnetic pole can be obtained by solving the above equations.

3 Optimization

The optimization objective of the electromagnet is to maximize the ratio of electromagnetic force to power consumption by optimally allocating the turns and currents of the constant-current coil and the regulation coil.Meanwhile, as the pole pitch of the electromagnet remains unchanged, the installation space is constrained, resulting in a limited cross-sectional area of the electromagnet coils.The optimization mathematical model of the electromagnet can be described as follows in Equation (11).

$$
\begin{cases}
\max(F / P) \\
s.t \begin{cases}
F_s + F_d - F_1 \geq 0 \\
P_s + P_d - P_1 \leq 0 \\
N_s S_s \leq 1.1 N_1 S_1 \\
N_d S_d \leq 1.1 N_1 S_1 \\
T_s \leq T_1 \\
T_d \leq T_1
\end{cases}
\end{cases} \tag{11}
$$

where P is the power loss of the electromagnet, and F is the electromagnetic force of the electromagnet. F_s, F_d, and F_1 represent the electromagnetic forces of the regulation coil, constant-current coil, and conventional electromagnet, respectively. P_s, P_d, and P_1 denote the power losses of the regulation coil, constant-current coil, and conventional electromagnet, respectively.N_s, N_d, and N_1 are the numbers of turns of the regulation coil, constant-current coil, and conventional electromagnet, respectively. S_s , S_d , and S_1 stand for the aluminum foil thicknesses adopted in the regulation coil, constant-current coil, and conventional electromagnet, respectively.T_s , T_d , and T_1 indicate the maximum internal temperatures of the pole for the regulation coil, constant-current coil, and conventional electromagnet, respectively.

The optimization analysis of the above mathematical model is carried out according to the following procedure:a set of values for the number of turns, current, and aluminum foil thickness of the regulation coil and constant-current coil is determined, and verified against the constraint conditions.Sets that fail to satisfy the constraints are eliminated.The valid set is compared with the previous one, and the set with lower power loss and larger electromagnetic force is retained for comparison with the next set. Finally, an optimal set of coil turns, current, and aluminum foil thickness is obtained.The parameters of the electromagnet under rated conditions before and after optimization are listed in Table 1.

Item	Turns	Rated current [A]	Rated electromagnetic air gap [mm]
Current suspended magnet	300	25	12.5
Regulation coil	165	23	12.5
Constant current coil	165	23	12.5

Table 1: The levitation magnet parameters before and after optimization.

4 Result

Based on the relevant parameters, finite element models of the electromagnet before and after optimization are established.The levitation force, power loss and temperature rise characteristics of the electromagnet are obtained through simulation, and the feasibility of the novel electromagnet scheme is analyzed.

4.1 Electromagnetic Force

Finite element models of the conventional electromagnet and the novel electromagnet are established.The variation of levitation force with current under different air gaps is calculated, and the levitation force–air gap–current characteristic curves of the electromagnet are obtained, as shown in Figure 10. It can be seen from the figure that within the operating current range of 0A~30 A for the conventional electromagnet, the electromagnetic force of the optimized electromagnet is significantly improved under the same regulation current.When the current exceeds 30 A, the electromagnetic force of the optimized electromagnet is lower than that of the conventional one. The conventional electromagnet exhibits a favorable linear region of levitation force at 20A~40 A,while the linear region of electromagnetic force for the optimized electromagnet ranges from 15 A to 45 A.The wider linear range is more conducive to electromagnetic regulation.

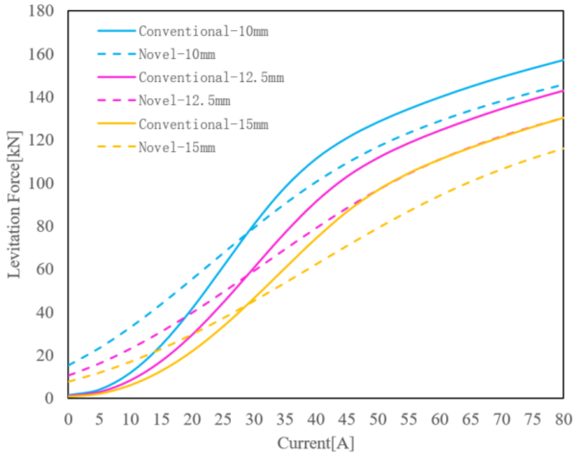

Figure 10: Force-gap-current curve.

The magnetic field of the magnet before and after optimization was analyzed in the case of a gap of 12.5mm. The working current of the magnet before optimization is 25A. After optimization, the working current of the constant current coil is 23A, and the working current of the regulation coil is 22.5A. The magnetic field distribution of the magnet is shown in Figure 11. The optimized magnetic pole and core have relatively uniform magnetic density. The magnetic field in most areas is between 1.0 and 1.6T. There was no significant magnetic saturation or large areas of low magnetic density.

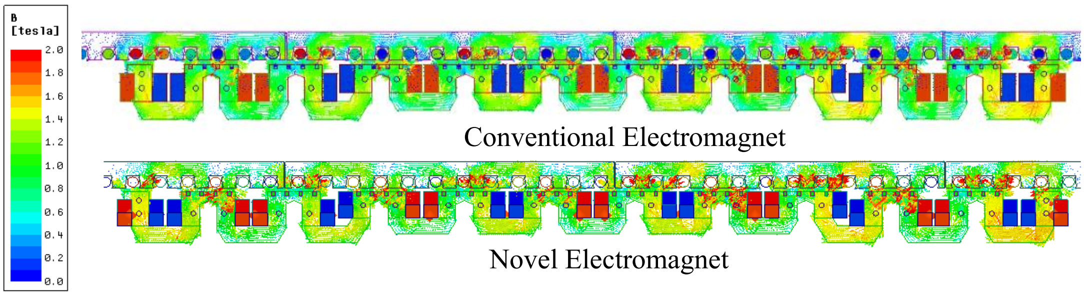

Figure 11: Magnet magnetic field cloud map.

4.2 Force-to-Power Ratio Characteristics

At an electromagnetic air gap of 12.5 mm, the ratio curves of electromagnetic force to power loss for the conventional and novel electromagnets are calculated and shown inFigure 12. It can be seen from the figure that when the operating current of the regulation coil exceeds 20 A, the force-to-power ratio of the novel electromagnet is higher than that of the conventional one, indicating that the novel electromagnet can generate greater levitation force per unit power consumption. For the conventional electromagnet at a 12.5 mm air gap and 25 A supply current, the force-to-power ratio is approximately 26.98 N/W.For the novel electromagnet at a 12.5 mm air gap, with a constant-current coil current of 23 A and a regulation coil current of 25 A, the force-to-power ratio is about 27.42 N/W, representing an improvement of approximately 1.7% compared with the conventional design. When the constant-current coil is supplied with 23 A and the regulation coil with 22.5 A, the force-to-power ratio reaches about 27.74 N/W, an increase of approximately 2.8% over the conventional scheme.

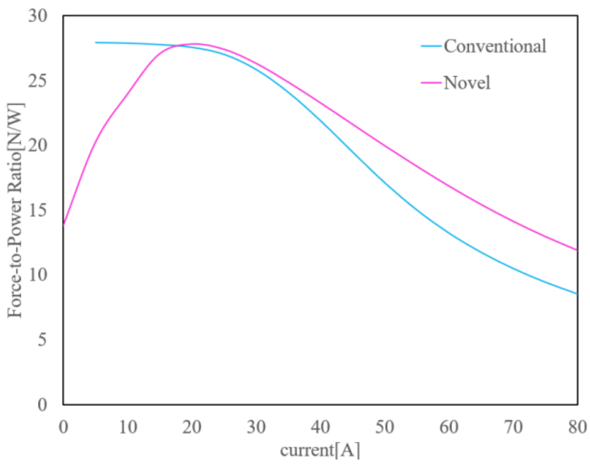

Figure 12: Power Loss-Electromagnetic Force Characteristics.

4.3 Temperature Characteristics

A magnetic pole temperature model is established to analyze the temperature variation laws of conventional and novel magnetic poles within the same duration. The results under no-wind conditions are shown in Figure 13, and those under wind conditions are shown in Figure 14. For the conventional electromagnet at a 12.5 mm electromagnetic air gap and 25 A rated current, the maximum internal temperature of the magnetic pole reaches 128.7 °C in approximately 60 minutes.For the novel electromagnet at a 12.5 mm air gap, with 23 A in the constant-current coil and 22.5 A in the regulation coil, the maximum internal temperature of the magnetic pole reaches 119 °C in about 60 minutes, representing a temperature rise reduction of 9.7 K compared with the conventional electromagnet.Under dynamic wind speed conditions, the temperature rise of the conventional electromagnet reaches 138 °C at 270 min, while that of the novel electromagnet is 111 °C, representing a reduction of 27 K.

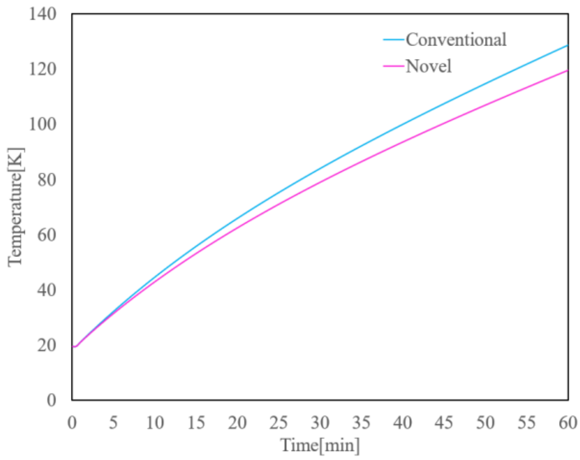

Figure 13: Static temperature rise characteristic curve.

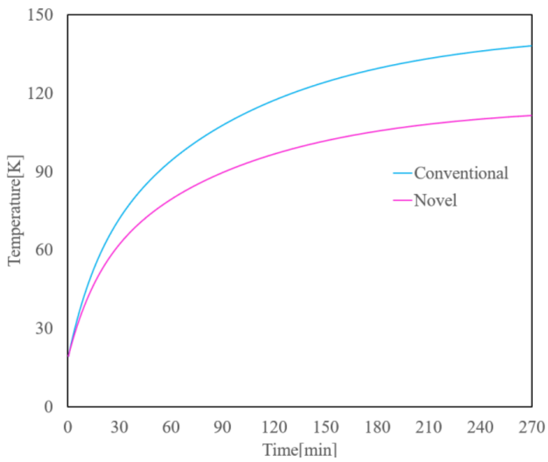

Figure 14: Dynamic temperature rise characteristics.

5 Conclusions and Contributions

In this paper, the coil on the electromagnet pole of a high-speed maglev system is divided into a regulation coil and a constant-current coil.The regulation coil is connected to the controller to adjust the electromagnetic force in real time, while the constant-current coil is connected to a constant-current source to provide the rated load capacity.By optimizing the turns and current ratio of the two coils, the electromagnet can generate a larger electromagnetic force within the operating current range of 0~30A.Near the rated operating point of the coil, the power consumption of the novel electromagnet is reduced.At the rated operating point, the force-to-power ratio is increased by 2.8%, and the temperature rise is reduced by 9.7 K under static no-wind conditions and by 27 K under dynamic wind conditions.

This optimal design fundamentally improves the energy efficiency and thermal characteristics of the high-speed maglev levitation electromagnet.While enhancing the load capacity, it effectively suppresses the coil temperature rise, delays the aging of insulation materials, and extends the service life of the electromagnet.It is of great significance for improving the long-term operational reliability, energy-saving performance, and overall system economy of high-speed maglev trains.

Acknowledgements

The authors would like thank National Key R&D Program of China under Grant (2023YFB4302500).

References

[1] J. Y. Xiong, Z. G.Deng, , "Research progress of high-speed maglev rail transit", Journal of Traffic and Transportation Engineering, 21, 177-198, 2021.

[2] Z. G. Deng, Z. X. Liu, H. T. Li and W. H. Zhang , "Development status and prospect of maglev train", Journal of Southwest Jiaotong University, 57, 455-474, 2022.

[3] Y. Y. Zheng, Q. F. Lu, Y. Zhou, L. F. Ju, "Force Performance Analysis of Long-Stator Linear Synchronous Motor Considering Air Gap Variation of Levitation and Guidance", Small & Special Electrical Machines, 52, 22-27, 2024.

[4] X. Liang, T.Y.Jiang, Y.Hong, J.B. Zhang, M.Jiang, Z.Y.Wang,"Vibration Response Analysis of Simply Supported Box Girder Bridge-Maglev Train in Accelerated Test of Changsha Maglev Express". Advances in Materials Science and Engineering, 9563747,2020.

[5] J. Q. Xu, C. Chen, Y. G. Sun, L. J.Rong, G. B. Lin,"Nonlinear Dynamic Characteristic Modeling and Adaptive Control of Low Speed Maglev Train", International Journal of Applied Electromagnetics and Mechanics, 62, 73-92, 2019.

[6] J. Ding, X. Yang, Z. Long, "Structure and control design of levitation electromagnet for electromagnetic suspension medium-speed maglev train", Journal of Vibration and Control, 25, 1179-1193, 2019.

[7] A. Chaban, Z. Lukasik, , M. Lis, A. Szafraniec, "Mathematical Modeling of Transient Processes in Magnetic Suspension of Maglev Trains", Energies, 13, 6642, 2020.
[8] L. B. Cui, G. T. Ma, Z. H. Su, J. Li, P. Feng, M. Guo, J. Zhao, J. Luo, "Partial Force Calculation and Structural Strength Analysis of Null-Flux Coil for Superconducting Electrodynamic Suspension Train", IEEE Transactions on Applied Superconductivity, 34, 1-10, 2024.
[9] J. Luo, L. B. Cui, Z. H. Su, Y. X. Li, J. Li, Z. X. Zhu, G. T. Ma, "Design Optimization of Null-Flux Superconducting Electrodynamic Suspension for Cost-Saving and Performance Improvement", IEEE/ASME Transactions on Mechatronics , 28, 3502-3512, 2023.
[10] Y. Sun, H. Qiang, L. Wang, W. Ji, A. Mardani, "A Fuzzy-Logic-System-Based Cooperative Control for the Multielectromagnets Suspension System of Maglev Trains With Experimental Verification", IEEE Transactions on Fuzzy Systems, 31, 3411-3422, 2023.
[11] Y. L. Xu, Z. L.Wang, G. Q. Li, S. W.Chen, Y. B. Yang, "High-speed running maglev trains interacting with elastic transitional viaducts", Engineering Structures, 183, 562-578, 2019.
[12] Y. He, J. Wu, G. Xie, X. Hong, Y. Zhang, "Data-driven relative position detection technology for high-speed maglev train", Measurement, 180, 109468, 2021.
[13] S. S. Ding, J. J. Sun, G. M. Deng, "Modeling and analysis of a linear generator for high-speed maglev train", IEEE Access, 9, 24637-24645, 2021.
[14] T. Zhang, D. Shen, S. Jiang, H. Xu, "Adaptive Fixed-Time Antilock Control of Levitation System of High-Speed Maglev Train", IEEE Transactions on Intelligent Vehicles, 27, 3394-3404, 2023.
[15] P. Schmid, G. Schneider, F.Dignath, X. Liang, P. Eberhard, "Static and Dynamic Modeling of the Electromagnets of the Maglev Vehicle Transrapid", IEEE Transactions on Magnetics, 57, 1-15, 2021.
[16] M. Zhang, W. H. Ma, T. Li, S. H.Luo, "Simulation of the Influence of Coil Connection mode on Levitation Control Performance", Journal of Mechanical Engineering, 55, 149-156, 2019.
[17] S. S. Ding, J. J. Sun, W. T. Han, "Modeling and analysis of a novel guidance magnet for high-speed maglev train", IEEE Access, 7, 133324-133334, 2019.
[18] Y. Zhang, G. M.Qing, Z. Y.Zhang, J. H. Li, H. G. Chen, "Calculation and Simulation of Propulsion Power Supply System for High-speed Maglev Train", in "Proceedings of the 2020 IEEE Vehicle Power and PropulsionConference (VPPC)",Spain,1-5 ,2020. doi:10.1109/VPPC50015. 2020. 9372979
[19] X. Q. Cao, Q. X. Ge, B. Zhang, J. Q. Zhu, M. T. Zhao, Y. X.Zheng, "Current Control Strategy of High-Speed Maglev Train Based on Sliding Mode", in "Proceedings of the 2021 13th International Symposium on Linear Drives for Industry Applications (LDIA)", IEEE, Wuhan, China, 1-5, 2021.doi:10.1109/LDIA49489.2021.9505735
[20] Schiefer, P., Kleikemper, O., & Holzapfel, F., "Modeling of Coupled Electric and Magnetic Circuits in Electromagnetic Suspension Vehicles", IEEE Transactions on Transportation Electrification, 11, 916-926, 2025.

[21] S. Wang, Q. Zhu,M. Zhang, Y. Q.Ni, "Gaussian Process Dynamic Modeling and Backstepping Sliding Mode Control for Magnetic Levitation System of Maglev Train", in "Proceedings of 2023 IEEE International Electric Machines & Drives Conference (IEMDC)", IEEE, San Francisco, CA, USA, 1-7, 2023. doi:10.1109/IEMDC54190.2023.10373624.

[22] S. Fu, Z. Deng, W. Han, X. Gao, Y. Zhou, "Modeling and Analysis of a Novel Levitation Magnet with Damping Coils for High-Speed Maglev Train", Sustainability, 16, 5247, 2024.

[23] S. Fu, Z. Deng, W. Han, D. Wu, "Modeling and Analysis of a Novel Levitation Magnet with Damping Coils for High-Speed Maglev Train", Sustainability, 16, 1-14, 2024.